# Delay-Phase Precoding for THz Massive MIMO with Beam Split

Jingbo Tan, Linglong Dai
Beijing National Research Center for Information Science and Technology, Department of Electronic Engineering, Tsinghua University, Beijing 100084, China

***Abstract*—Benefiting from tens of GHz bandwidth, Terahertz (THz) communications has been considered as one of the promising technologies for the future 6G wireless communications. To compensate the serious attenuation in THz band and avoid huge power consumption, massive multiple input multiple output (MIMO) with hybrid precoding is widely considered. However, the traditional phase-shifter (PS) based hybrid precoding architecture cannot cope with the effect of beam split in THz communications, which means that the path components of THz channel split into different spatial directions at different subcarrier frequencies, leading serious array gain loss. In this paper, we first point out the seriousness of beam split effect in THz massive MIMO by analyzing the array gain loss caused by the beam split effect. To compensate this array gain loss, we propose a new hybrid precoding architecture called delay-phase precoding (DPP). In the proposed DPP, a time delay (TD) network is introduced between radio-frequency chains and the traditional PS network, which converts phase-controlled analog precoding into delay-phase controlled analog precoding. When carrying out precoding, the time delays in the TD network are dedicatedly designed to generate frequency-dependent beams which are aligned with the spatial directions over the whole bandwidth. Thanks to the joint control of delay and phase, the proposed DPP can significantly alleviate the beam split effect. Simulation results reveal that the proposed DPP can generate beams with the near-optimal array gain over the whole bandwidth, and achieve the near-optimal achievable rate performance.**

***Index Terms*—THz communications, massive MIMO, hybrid precoding, beam split**

## I. Introduction

Terahertz (THz) communications has been considered as a promising technology to support the very high data rate in the future 6G wireless communications, since it can provide tenfold increase in the bandwidth [1]. Compared to the typical 2 GHz bandwidth in the millimeter (mmWave) band (30-300 GHZ) [2], the THz band (0.1-10 THz) is able to provide tens of GHz bandwidth [1]. However, as the carrier frequency increases, the THz signals suffer from more severe attenuation, which becomes a vital problem in THz communications [3]. Massive multiple input multiple output (MIMO), which utilizes a large antenna array to offer the directional array gain, can compensate such severe attenuation. Consequently, THz massive MIMO is very promising for future 6G wireless communications [4]. Similar to mmWave massive MIMO in 5G, hybrid precoding is attractive for THz massive MIMO to relieve the huge power consumption of the THz radio-frequency (RF) chains [5]. The main idea of hybrid precoding is to decompose the high-dimensional fully-digital precoder into an analog beamformer realized by phase-shifters (PSs) and a digital precoder, with a significantly reduced number of RF chains [6]. Thanks to the sparsity of the THz channel [7], a small number of RF chains is able to fully achieve the mutiplexing gain of massive MIMO [6], [8].

In existing hybrid precoding architecture [8], the analog beamformer consists of directional beams, which are aligned with the spatial directions of the channel path components, to realize the full array gain. This is feasible for the narrowband systems. However, for the wideband mmWave systems, the spatial directions are different at different subcarrier frequencies, which leads to the obvious array gain loss since the traditional analog beamformer is realized by *frequency-independent* PSs [8]. To deal with this effect called beam squint, several methods has been proposed in mmWave massive MIMO systems [9]–[12]. Specifically, in [9], [10], the analog beamformer and digital precoder are jointly optimized to achieve the optimal achievable rate. In [11], [12], new analog beamforming codebooks with wider beam width are proposed to avoid the array gain decrease.

These methods [9]–[12] can improve the achievable rate performance, as the path components only slightly squint and the array gain loss is limited in mmWave systems. However, due to the much larger bandwidth of THz signals, the path components split into totally separated spatial directions at different subcarrier frequencies, which makes these methods [9]–[12] invalid for THz communications. Moreover, the phase-controlled beams generated by the frequency-independent PSs can only realize high array gain around the central frequency, while suffer from the severe array gain loss at most subcarrier frequencies. We call this effect as beam split effect in THz communications. The beam split effect will result in a serious achievable rate loss, and counteract the achievable rate gain benefiting from the bandwidth increase. However, to our best knowledge, the beam split effect in THz massive MIMO has not been pointed out, and there are no corresponding solutions.

To mitigate the beam split effect in THz massive MIMO, in this paper, we propose a new hybrid precoding architecture call delay-phase precoding (DPP). Specifically, we first point out the seriousness of the beam split in wideband THz communications through analysis. Then, we propose a new hybrid precoding architecture called DPP. In the proposed DDP, a time delay (TD) network, is introduced between the digital precoder and traditional analog beamformer. Through the TD network, DPP can realize the jointly delay-phase controlled beamformer. Unlike the traditional phase-controlled beamformer, DPP can realize the *frequency-dependent* beamforming, which can significantly alleviate the beam split effect. When carraying out precoding, the traditional PSs still generate beams towards spatial directions at the central frequency,

978-1-7281-0962-6/19/$31.00 ©2019 IEEE

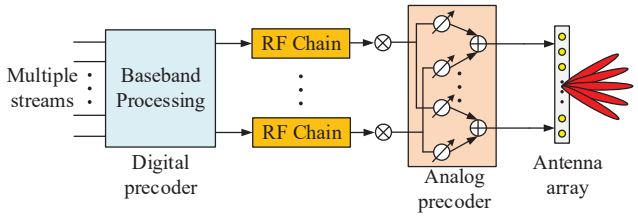


Fig. 1. Typical hybrid precoding structure.

while the time delays in the TD network are dedicatedly designed to make the beams aligned with the spatial directions over the whole bandwidth. Simulation results verify that the proposed DDP can achieve the near-optimal achievable rate.

*Notation:* Lower-case and upper-case boldface letters represent vectors and matrices, respectively; $(\cdot)^T$ and $(\cdot)^H$ denote the transpose and conjugate transpose, respectively; $\mathbf{H}_{[i,j]}$ denotes the element of matrix $\mathbf{H}$ at the $i$-th row and the $j$-th column; $\mathbb{E}(\cdot)$ denotes the expectation; $|\cdot|$ denotes the absolute operator; $\mathbf{I}_N$ represents the identity matrix of size $N \times N$; $\mathrm{diag}(\mathbf{A})$ denotes block diagonal matrix where each column of $\mathbf{A}$ represents the diagonal elements. $\mathcal{CN}(\mu, \mathbf{\Sigma})$ and $\mathcal{U}(a, b)$ denote the Gaussian distribution with mean $\mu$ and covariance $\mathbf{\Sigma}$, and the uniform distribution between $a$ and $b$, respectively.

## II. System model

We consider a THz massive MIMO system with conventional hybrid precoding as shown in Fig. 1. The base station (BS) employs an $N_t$-antenna uniform linear array and $N_{RF}$ radio-frequency chains. An $N_r$-antenna user is served and $N_s$ data streams are transmitted simultaneously ($N_s = N_r \leq N_{RF} \ll N_t$). To realize reliable wideband transmission, we adopt orthogonal frequency division multiplexing (OFDM) with $M$ subcarriers. The received $N_r$-stream signal at the $m$-th subcarrier $\mathbf{y}_m \in \mathcal{C}^{N_r \times 1},\ m = 1, 2, \cdots, M$ is

$$\mathbf{y}_m = \mathbf{H}_m^H \mathbf{A} \mathbf{D}_m \mathbf{s}_m + \mathbf{n}_m, \tag{1}$$

where $\mathbf{H}_m \in \mathcal{C}^{N_t \times N_r}$ denotes the channel at the $m$-th subcarrier, $\mathbf{A} \in \mathcal{C}^{N_t \times N_{RF}}$ is the analog beamformer which is the same for all the subcarriers due to the use of traditional frequency-independent PSs [8] with restriction $|\mathbf{A}_{[i,j]}| = \frac{1}{\sqrt{N_t}}$, $\mathbf{D}_m \in \mathcal{C}^{N_{RF} \times N_s}$ is the digital precoder at the $m$-th subcarrier satisfying $\|\mathbf{A}\mathbf{D}_m\|_F = \rho$, where $\rho$ is the transmission power, and $\mathbf{n}_m \in \mathcal{C}^{N_r \times 1}$ denotes the additive white Gaussian noise (AWGN) at the $m$-th subcarrier following the distribution $\mathbf{n}_m \sim \mathcal{CN}(0, \sigma^2 \mathbf{I}_{N_r})$ with $\sigma^2$ presenting the noise power.

For the THz channel, we consider a widely utilized wideband ray-based channel model [7]. Denote $f_c$ as the central frequency and $f$ as the bandwidth. Then, the frequency at the $m$-th subcarrier is $f_m = f_c + \frac{f}{M}(m - 1 - \frac{M-1}{2}), m = 1, 2, \cdots, M$. For the $m$-th subcarrier, the channel can be presented as

$$\mathbf{H}_m = \sum_{l=1}^{L} g_l e^{-j2\pi\tau_l f_m} \mathbf{f}_t(\theta_{l,m}) \mathbf{f}_r(\phi_{l,m})^H, \tag{2}$$

where $L$ denotes the number of resolvable paths, $g_l$ and $\tau_l$ represents the path gain and path delay of the $l$-th path, $\theta_{l,m}, \phi_{l,m} \in [-1, 1]$ denote the spatial direction of the transmitter and the receiver of the $l$-th path and $m$-th subcarrier, respectively, and $\mathbf{f}_t(\theta_{l,m})$, $\mathbf{f}_r(\phi_{l,m})$ are the array response at the transmitter and receiver, e.g., $\mathbf{f}_t(\theta_{l,m})$ can be presented as

$$\mathbf{f}_t(\theta_{l,m}) = \frac{1}{\sqrt{N_t}} \left[1, e^{j\pi\theta_{l,m}}, e^{j\pi 2\theta_{l,m}}, \cdots, e^{j\pi(N_t-1)\theta_{l,m}}\right]^T. \tag{3}$$

In (3), the spatial directions are the directions of the paths in the spatial domain, which are determined by the physical propagation direction and the subcarrier frequency, e.g., for the spatial direction of the transmitter, we have $\theta_{l,m} = 2d\frac{f_m}{c}\sin\gamma_l$, where $c$ denotes the light speed, $\gamma_l \in [-\pi/2, \pi/2]$ is the physical propagation direction of the $l$-th path, $d$ is the fixed antenna spacing with $d = \frac{c}{2f_c}$.

## III. Beam Split

In this section, we will point out the beam split effect with the serious array gain degradation. We first consider the $l$-th path component with spatial direction $\theta_{l,m}$ in THz massive MIMO channel without loss of generality. Usually, one column of the analog beamformer $\mathbf{a}_l = \mathbf{A}_{[:,l]}$, is used to generate a beam on the $l$-th path's spatial direction at $f_c$ by setting $\mathbf{a}_l = \mathbf{f}_t(\theta_{l,c})$ [8], where $\theta_{l,c} = 2d\frac{f_c}{c}\sin\gamma_l$. Thus, the array gain of $\mathbf{a}_l$ on the spatial direction $\theta_{l,c}$ is

$$|\eta(\mathbf{a}_l, \theta_{l,c})| = \left|\mathbf{f}_t(\theta_{l,c})^H \mathbf{a}_l\right| = \left|\mathbf{f}_t(\theta_{l,c})^H \mathbf{f}_t(\theta_{l,c})\right| = 1, \tag{4}$$

which means by setting $\mathbf{a}_l = \mathbf{f}_t(\theta_{l,c})$, $\mathbf{a}_l$ can achieve highest array gain at $f_c$. Thus, the narrowband systems can enjoy highest array gain over the whole bandwidth due to $f_m \approx f_c$.

However, in wideband systems, the difference between $f_m$ and $f_c$ cannot be ignored. Therefore, the path components have different spatial directions at different subcarriers as

$$\theta_{l,m} = \frac{f_m}{f_c}\theta_{l,c} = \xi_m \theta_{l,c}, . \tag{5}$$

where $\xi_m = \frac{f_m}{f_c}$ is the relative frequency. In THz communications, the path components may even split into significantly different spatial directions at different subcarriers due to the wide bandwidth. This beam split effect causes serious array gain loss, which can be explained by **Lemma 1**.

**Lemma 1.** *When $|(\xi_m - 1)\theta_{l,m}| \geq \frac{1}{N_t}$, the ratio $\zeta$ between the array gain of $\mathbf{a}_l$ on spatial direction $\theta_{l,m}$ and that on the central spatial direction $\theta_{l,c}$ is*

$$\zeta = \frac{|\eta(\mathbf{a}_l, \theta_{l,m})|}{|\eta(\mathbf{a}_l, \theta_{l,c})|} \leq \frac{1}{N_t \sin\frac{3\pi}{2N_t}}, \tag{6}$$

*Proof:* The array gain of $\mathbf{a}_l$ on the spatial direction $\theta \in [-1, 1]$ can be denoted as $|\eta(\mathbf{a}_l, \theta)| = \left|\mathbf{f}_t(\theta)^H \mathbf{a}_l\right|$. Then, the array gain $\eta(\mathbf{a}_l, \theta_{l,m})$ satisfies

$$\begin{aligned}\eta(\mathbf{a}_l, \theta_{l,m}) = \mathbf{f}_t(\theta_{l,m})^H \mathbf{f}_t(\theta_{l,c}) &\overset{(a)}{=} \frac{1}{N_t}\sum_{n=0}^{N_t-1} e^{-jn\pi(\xi_m-1)\theta_{l,c}} \\ &\overset{(b)}{=} \frac{\sin\frac{N_t\pi}{2}(\xi_m-1)\theta_{l,c}}{N_t \sin\frac{\pi}{2}(\xi_m-1)\theta_{l,c}} e^{j\frac{(N_t-1)\pi}{2}(\xi_m-1)\theta_{l,c}},\end{aligned} \tag{7}$$

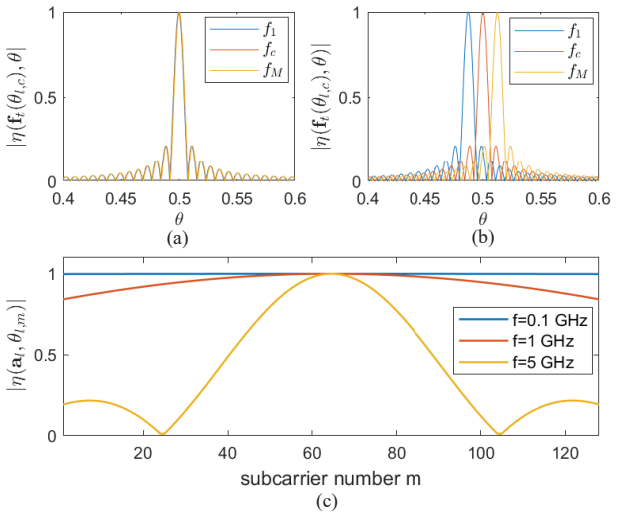


Fig. 2. (a) beam pattern of $\mathbf{f}_t(\theta_{l,c})$ in narrowband channel; (b) beam pattern of $\mathbf{f}_t(\theta_{l,c})$ in wideband channel; (c) array gain performance of $\mathbf{a}_l$.

where (a) comes from (8) and (b) comes from the equation $\Sigma_{n=0}^{N-1} e^{-jn\pi\alpha} = \frac{\sin\frac{N_t\pi}{2}\alpha}{N_t\sin\frac{\pi}{2}\alpha} e^{j\frac{(N-1)\pi}{2}\alpha}$. Thus, the array gain of $\mathbf{a}_l$ on the spatial direction $\theta_{l,m}$ is

$$|\eta(\mathbf{a}_l,\theta_{l,m})| = \frac{1}{N_t}|\Xi_{N_t}((\xi_m-1)\theta_{l,c})|, \tag{8}$$

where $\Xi_{N_t}(x) = \frac{\sin\frac{N_t\pi}{2}x}{\sin\frac{\pi}{2}x}$ is the Dirichlet sinc function, where $\Xi_{N_t}(0) = N_t$ is the maximum and the value of $\Xi_{N_t}(x)$ decreases sharply as $|x|$ increases [13]. Specifically, the array gain ratio between the spatial direction $\theta_{l,m}$ and $\theta_{l,c}$ is

$$\zeta = \frac{|\eta(\mathbf{a}_l,\theta_{l,m})|}{|\eta(\mathbf{a}_l,\theta_{l,c})|} = \frac{1}{N_t}|\Xi_{N_t}((\xi_m-1)\theta_{l,c})|. \tag{9}$$

When $|(\xi_m-1)\psi_l| \geq \frac{2}{N_t}$, according to the power-focusing property of $\Xi(x)$ [13], we have

$$\zeta \leq \frac{1}{N_t\sin\frac{3\pi}{2N_t}}, \tag{10}$$

which completes the proof. ■

According to **Lemma 1**, we can see that since the spatial directions change from $\theta_{l,c}$ to $\theta_{l,m}$ at different subcarrier frequencies, the frequency-independent beam $\mathbf{a}_l$ which is aligned with $\theta_{l,c}$ cannot achieve the highest array gain. Moreover, when the bandwidth $\xi_m$ becomes larger in THz communications, $\mathbf{a}_l$ causes severe array gain loss because the path components are totally splited into different spatial directions and larger number of subcarriers satisfy $|(\xi_m-1)\psi_l| \geq \frac{2}{N_t}$. E.g., Fig. 2 (a) and (b) illustrates the beam pattern $|\eta(\mathbf{f}_t(\theta_{l,c}),\theta)|$ with parameters $f_c = 100$ GHz, $\theta_{l,c} = 0.5$, $N_t = 256$ and $M = 128$. The narrowband and wideband case with $f = 0.1$ GHz and $f = 5$ GHz are shown in Fig. 2 (a) and (b), respectively. We can observe from Fig. 2 (b) that the spatial directions obviously separate from $\theta_{l,c}$ in wideband case at $f_1$ and $f_M$. In Fig. 2 (c), the array gain of $\mathbf{a}_l$ at different subcarriers is shown. We can see that as the bandwidth increases, the array gain loss becomes larger. When $m \leq 25$ or $m \geq 103$, $|(\xi_m-1)\psi_l| \geq \frac{2}{N_t}$ in $f = 5$ GHz case, which means more than $40\%$ subcarriers suffer nearly $80\%$ array gain loss according to (10). Such a serious array gain loss will lead to serious achievable rate degradation, which is not acceptable in the future THz communications. However, the existing hybrid precoding architecture cannot solve this problem. To this end, in the next section we will propose a new hybrid precoding architecture called DPP.

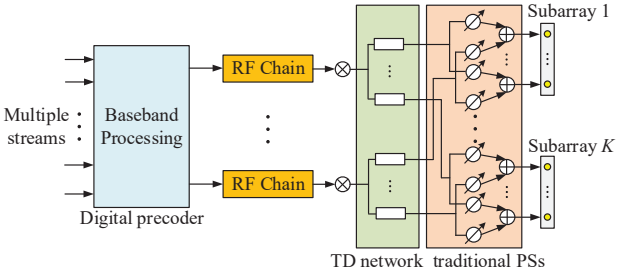


Fig. 3. The proposed DPP structure.

## IV. Delay-Phase Precoding

As discussed in III, due to the beam split effect, the frequency-independent beamformer cannot generate beams aligned with frequency-dependent spatial directions, which is the main reason of the severe array gain loss. To solve this problem, we propose a new precoding architecture called DPP. The proposed DPP architecture is shown in Fig. 3. In the DPP, we introduce a TD network between the digital precoder and the traditional analog beamformer. The proposed DPP converts the traditional phase-controlled beamformer into jointly delay-phase controlled beamformer, which can realize frequency-dependent beamforming. Specifically, each RF chain is connected to $K$ TD elements and each TD element is connected to $P = N_t/K$ traditional frequency-independent PSs in a sub-connected manner. The TD network, as a new layer of precoding, can realize frequency-dependent phase shifts through time delays, e.g., $-2\pi f_m t$ phase shift by time delay $t$ at $f_m$. Therefore, the received signal at the $m$-th subcarrier can be denoted as

$$\mathbf{y}_m = \mathbf{H}_m^H\mathbf{A}_u\mathbf{A}_m^{TD}\mathbf{D}_m\mathbf{s}_m + \mathbf{n}_m, \tag{11}$$

where $\mathbf{A}_m^{TD} \in \mathcal{C}^{KN_{RF}\times N_{RF}}$ denotes the frequency-dependent phase shifts realized by TD network, and satisfies

$$\mathbf{A}_m^{TD} = \mathrm{diag}([e^{-j2\pi f_m\mathbf{t}_1},\cdots,e^{-j2\pi f_m\mathbf{t}_{N_{RF}}}]), \tag{12}$$

where $\mathbf{t}_l \in \mathcal{C}^{K\times 1} = [t_{l,1}, t_{l,2},\cdots,t_{l,K}]^T$ denotes the time delays realized by $K$ TD elements for the $l$-th beam. The original analog beamformer $\mathbf{A}$ in (1) is correspondingly reshaped as $\mathbf{A}_u = [\mathbf{A}_{u,1},\mathbf{A}_{u,2},\cdots,\mathbf{A}_{u,N_{RF}}]$ with

$$\mathbf{A}_{u,l} = \mathrm{diag}([\widetilde{\mathbf{a}}_{l,1},\widetilde{\mathbf{a}}_{l,2},\cdots,\widetilde{\mathbf{a}}_{l,K}]), \tag{13}$$

where $\widetilde{\mathbf{a}}_{l,k} \in \mathcal{C}^{P\times 1}$ denotes the beamforming vector of $P$ frequency-independent PSs connected to the $k$-th TD element for the $l$-th beam.

The next question is how to utilize the time delay realized by the TD network to mitigate the beam split effect. Con-

sidering $\bar{\mathbf{a}}_{l,m}$ as the $l$-th column of $\mathbf{A}_u\mathbf{A}_m^{TD}$ with $\bar{\mathbf{a}}_{l,m} = \mathbf{A}_{u,l}e^{-j2\pi f_m \mathbf{t}_l}$, the array gain of $\bar{\mathbf{a}}_{l,m}$ satisfies **Lemma 2**.

**Lemma 2.** *When* $\widetilde{\mathbf{a}}_{l,k}$ *satisfies* $[\widetilde{\mathbf{a}}_{l,1}^T, \widetilde{\mathbf{a}}_{l,2}^T, \cdots, \widetilde{\mathbf{a}}_{l,K}^T]^T = \mathbf{f}_t(\theta_{l,c})$ *and* $e^{-j2\pi f_m \mathbf{t}_l} = \left[1, e^{j\pi\beta}, \cdots, e^{j\pi(K-1)\beta}\right]^T$, $\bar{\mathbf{a}}_{l,m}$ *is aligned with the spatial direction* $\psi_l$ *as*

$$\psi_l = \arg\max_{\theta} |\eta(\bar{\mathbf{a}}_{l,m}, \theta)| = \theta_{l,c} + \frac{\beta}{P}. \tag{14}$$

*where* $\beta \in [-1, 1]$ *with array gain* $|\eta(\bar{\mathbf{a}}_{l,m}, \psi_l)| = \frac{K}{N_t}\Xi_P(\frac{\beta}{P})$.

*Proof:* The array gain of $\bar{\mathbf{a}}_{l,m}$ on the spatial direction $\theta$ can be represented as $|\eta(\bar{\mathbf{a}}_{l,m}, \theta)| = |\mathbf{f}_t(\theta)^H \bar{\mathbf{a}}_{l,m}|$. With $[\widetilde{\mathbf{a}}_{l,1}^T, \widetilde{\mathbf{a}}_{l,2}^T, \cdots, \widetilde{\mathbf{a}}_{l,K}^T]^T = \mathbf{f}(\theta_{l,c})$ and $e^{-j2\pi f_m \mathbf{t}_l} = \left[1, e^{j\pi\beta}, e^{j\pi 2\beta}, \cdots, e^{j\pi(K-1)\beta}\right]^T$, we have

$$\eta(\bar{\mathbf{a}}_{l,m}, \theta) = \frac{1}{N_t}\sum_{k=1}^{K}\sum_{p=1}^{P} e^{j\pi[(k-1)P+(p-1)]\theta_{l,c}} e^{j\pi(k-1)\beta} \times e^{-j\pi[(k-1)P+(p-1)]\theta}. \tag{15}$$

By seperating the summation on $K$ and $P$, we have

$$\eta(\bar{\mathbf{a}}_{l,m}, \theta) = \frac{1}{N_t}\sum_{k=1}^{K} e^{j\pi(k-1)[P(\theta_{l,c}-\theta)+\beta]} \times \sum_{p=1}^{P} e^{j\pi(p-1)(\theta_{l,c}-\theta)}. \tag{16}$$

Then, we can transform the summation as

$$|\eta(\bar{\mathbf{a}}_{l,m}, \theta)| = \frac{1}{N_t}|\Xi_K(P(\theta_{l,c}-\theta)+\beta)\Xi_P(\theta_{l,c}-\theta)|. \tag{17}$$

We can see that the array gain of $\bar{\mathbf{a}}_l$ is the product of two Dirichlet sinc function. For the $\Xi_K(P(\theta_{l,c}-\theta)+\beta)$, the maximum point is $\psi_{K,max} = \theta_{l,c}+\frac{\beta}{P}$ by setting $P(\theta_{l,c}-\theta)+\beta = 0$, and the main lobe width of $\Xi_K(P(\theta_{l,c}-\theta)+\beta)$ is $\frac{4}{N_t}$. Similarly for $\Xi_P(\theta_{l,c}-\theta)$, the maximum point is $\psi_{P,max} = \theta_{l,c}$ and the main lobe width is $\frac{4}{P}$. Considering that $\beta \in [-1, 1]$, we have, $\psi_{K,max} \in [\theta_{l,c}-\frac{1}{P}, \theta_{l,c}+\frac{1}{P}]$, which means that the maximum point of $\Xi_K(P(\theta_{l,c}-\theta)+\beta)$ locates in the main lobe of $\Xi_P(\theta_{l,c}-\theta)$ with range of $[\theta_{l,c}-\frac{2}{P}, \theta_{l,c}+\frac{2}{P}]$. Then, considering that the main lobe width of $\Xi_P(\theta_{l,c}-\theta)$ is $K$ times wider than $\Xi_K(P(\theta_{l,c}-\theta)+\beta)$, the variation range of $\Xi_P(\theta_{l,c}-\theta)$ in the main lobe of $\Xi_K(P(\theta_{l,c}-\theta)+\beta)$ is much smaller than the variation range of $\Xi_K(P(\theta_{l,c}-\theta)+\beta)$. Therefore, the maximum value of $|\eta(\bar{\mathbf{a}}_{l,m}, \theta)|$ can be approximately seen as decided by $\Xi_K(P(\theta_{l,c}-\theta)+\beta)$, which means

$$\psi_l = \arg\max_{\theta} |\eta(\bar{\mathbf{a}}_{l,m}, \theta)| = \psi_{K,max} = \theta_{l,c} + \frac{\beta}{P}, \tag{18}$$

which is also shown in Fig. 4. Then, the array gain $|\eta(\bar{\mathbf{a}}_{l,m}, \theta)|$ can be denoted by substituting (18) into (17) as

$$|\eta(\bar{\mathbf{a}}_{l,m}, \theta)| = \frac{1}{N_t}|\Xi_K(0)\Xi_P(\theta_{l,c}-\psi_l)| = \left|\frac{K}{N_t}\Xi_P(\frac{\beta}{P})\right|, \tag{19}$$

which completes the proof. ■

We can notice that a small phase shift $\beta$ provided by time delay can change the spatial direction of the original beam $\mathbf{f}_t(\theta_{l,c})$, from **Lemma 2**. Hence, the design of $\bar{\mathbf{a}}_{l,m}$ in the DPP is converted to designing the time delay that should be provided by the TD network, while the traditional PSs network still perform beamforming on the spatial direction $\theta_{l,c}$ as $[\widetilde{\mathbf{a}}_{l,1}^T, \widetilde{\mathbf{a}}_{l,2}^T, \cdots, \widetilde{\mathbf{a}}_{l,K}^T]^T = \mathbf{f}_t(\theta_{l,c})$. Specifically, the beam split can be compensated by setting $\beta$ satisfying $\psi_l = \theta_{l,m}$, which makes the spatial direction change from $\theta_{l,c}$ to $\theta_{l,m}$ at frequency $f_m$. Denoting $\bar{\beta}_{l,m}$ as the phase shift that the TD network should achieve to compensate the beam split at frequency $f_m$ for the $l$-th beam, we have

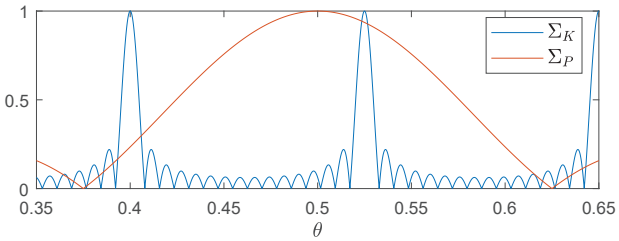


Fig. 4. The figure of Dirichlet sinc functions, where $\Xi_K$ denotes $|\frac{1}{K}\Xi_K(P(\theta_{l,c}-\theta)+\beta)|$ and $|\Xi_P|$ denotes $|\frac{1}{P}\Xi_P(\theta_{l,c}-\theta)|$.

$$\bar{\beta}_{l,m} = (\xi_m - 1)P\theta_{l,c}. \tag{20}$$

According to **Lemma 2** and (20), for the $l$-th beam, the time delays realized by $K$ TD elements should satisfy

$$e^{-j2\pi f_m \mathbf{t}_l} = \left[1, e^{j\pi\bar{\beta}_{l,m}}, e^{j\pi 2\bar{\beta}_{l,m}}, \cdots, e^{j\pi(K-1)\bar{\beta}_{l,m}}\right]^T. \tag{21}$$

Notice that for $f_c$, the required phase shift should be $\bar{\beta}_{c,l} = 0$. Thus, the time delays in $\mathbf{t}_l$ should be integer multiply of the period of $f_c$, to maintain the beam towards the spatial direction $\theta_{l,c}$. Under this point and (21), the time delay vector $\mathbf{t}_l$ should be set as $\mathbf{t}_l = [0, s_l T_c, 2s_l T_c, \cdots, (K-1)s_l T_c]^T$, where $T_c$ is the period of the carrier frequency $f_c$, and $s_l$ denotes the number of periods that should be delayed for the $l$-th beam. Thus, $s_l$ should satisfy

$$-2\pi f_m s_l T_c + 2\pi s_l = \pi\bar{\beta}_{m,l}, \tag{22}$$

where $2\pi s_l$ is to make the left side of (22) belong to $[-\pi, \pi]$, as the range of $\pi\bar{\beta}_{m,l}$ is also $[-\pi, \pi]$. Then, substituting $T_c = \frac{1}{f_c}$, $\xi_m = \frac{f_m}{f_c}$ and (20) into (22), we have

$$s_l = -\frac{P\theta_{l,c}}{2}. \tag{23}$$

Notice that in (23), the periods number $s_l$ is decided by $P$ and spatial direciton $\theta_{l,c}$ at $f_c$, and has no relationship with frequency $\xi_m$. This means that an identical time delay can compensate the beam split at all the subcarriers. Considering that $s_l$ is an integer and the time delays $t_{l,i}$ should be larger than 0, a small modification of (23) should be operated. Thus, the time delay of $i$-th TD element $t_{l,i}$ can be denoted as

$$t_{l,i} = \begin{cases} (K-1+i)\lfloor -\frac{P\theta_{l,c}}{2} \rceil T_c, & \theta_{l,c} > 0, \\ i\lfloor -\frac{P\theta_{l,c}}{2} \rceil T_c, & \theta_{l,c} \le 0, \end{cases} \tag{24}$$

where $(K-1)sT_c$ has been added to each time delays to make $t_{l,i}$ larger than 0 when $\theta_{l,c} > 0$, which guarantees that the phase shift is equal to $\bar{\beta}_{m,l}$.

**Algorithm 1** Hybrid precoding for the proposed DPP.

**Inputs:**

Channel $\mathbf{H}_m$; Spatial directions $\theta_{l,c}$;

**Output:**

Hybrid precoder $\mathbf{A}_u$, $\mathbf{A}_m^{TD}$ and $\mathbf{D}_m$;

1: **for** $l \in \{1, 2, \cdots, N_{RF}\}$ **do**
2: Generate $\mathbf{A}_{u,l}$ by $[\widetilde{\mathbf{a}}_{l,1}, \widetilde{\mathbf{a}}_{l,2}, \cdots, \widetilde{\mathbf{a}}_{l,K}]^T = \mathbf{f}_t(\theta_{l,c})$;
3: $s_l = -\frac{P\theta_{l,c}}{2}$;
4: $t_{l,i} = \begin{cases} (K-1+i)\lfloor s_l \rceil T_c, & \theta_{l,c} > 0 \\ i\lfloor s_l \rceil T_c, & \theta_{l,c} \le 0 \end{cases}$;
5: $\mathbf{t}_l = [t_{l,1}, t_{l,2}, \cdots, t_{l,K}]$;
6: **end for**
7: $\mathbf{A}_u = [\mathbf{A}_{u,1}, \mathbf{A}_{u,2}, \cdots, \mathbf{A}_{u,N_{RF}}]$;
8: **for** $m \in \{1, 2, \cdots, M\}$ **do**
9: $\mathbf{A}_m^{TD} = \mathrm{diag}([e^{-j2\pi f_m \mathbf{t}_1}, \cdots, e^{-j2\pi f_m \mathbf{t}_{N_{RF}}}])$;
10: $\mathbf{H}_{m,eq} = \mathbf{H}_m^H \mathbf{A}_u \mathbf{A}_m^{TD}$;
11: $\mathbf{D}_m = \mu \mathbf{V}_{m,eq,[:,1:N_{RF}]}, \mathbf{H}_{m,eq} = \mathbf{U}_{m,eq}\mathbf{\Sigma}_{m.eq}\mathbf{V}_{m,eq}^H$
12: **end for**
13: **return** $\mathbf{A}_u$, $\mathbf{A}_m^{TD}$ and $\mathbf{D}_m$.

Therefore, the DPP structure can compensate for the beam split by setting $t_{l,i}$ as (24) and $\mathbf{t}_l = [t_{l,1}, t_{l,2}, \cdots, t_{l,K}]^T$ for the $l$-th beam. Based on the deriviation above, we propose a hybrid precoding method for the DDP structure. Its key idea is to generate beams towards the spatial directions $\theta_{l,c}$ by frequency-independent PSs and compensate fthe beam split effect by the TD network, whose pseudo-code is illustrated in **Algorithm 1**. We assume that the BS knows the channel $\mathbf{H}_m$ and the spatial directions $\theta_{l,c}$, which can be obtained by efficient channel estimation scheme [14]. Without lossing generality, we assume that the spatial directions are sorted based on the path gains as $|g_1| > |g_2| > \cdots > |g_L|$. In **Algorithm 1**, the analog precoder for the $l$-th beam $\mathbf{A}_{u,l}$ is firstly calculated in step 2 to generate beams towards spatial direction $\theta_{l,c}$. Then, the time delays by $K$ TD elements are generated in step 3, 4 and 5, where the beams direction are changed from $\theta_{l,c}$ to $\theta_{l,m}$ at $f_m$. After that, the analog beamformer $\mathbf{A}_u$ and $\mathbf{A}_m^{TD}$ are generated in step 7 and 9. Finally, the digital precoder $\mathbf{D}_m$ is calculated based on the equivalent channel $\mathbf{H}_{m,eq}$ by traditional singular value decomposition (SVD) precoding [2] in step 10 and 11, where $\mu$ is the power normalization coefficient. Through **Algorithm 1**, the DPP can achieve near-optimal achievable rate, since each beam is aligned with the spatial direction at all the subcarriers by time delays, which will be verified in V by simulation results.

Due to the huge power consumption and high hardware complexity of TD elements [15], an important problem in the proposed DPP is that how many TD elements are sufficient to mitigate the beam split effect at all the subcarriers. In the previous deriviation, we have ignored that the phase shift $\bar{\beta}_{l,m}$ has a range restriction as $\bar{\beta}_m \in [-1, 1]$. Thus, to compensate for the beam split at all the subcarriers, $P$ should satisfy $-1 \le (\xi_m - 1)P\psi_l \le 1$. Recalling that $\psi_l \in [-1, 1]$, $\frac{f_1}{f_c} \le \xi_m \le \frac{f_M}{f_c}$ and $K = N_t/P$, we have

$$K \ge (\frac{f_M}{f_c} - 1)N_t. \tag{25}$$

From (25), we can observe that $K$ increases linearly with the relative bandwidth $f_M/f_c$. Since the relative bandwidth is usually limited, e.g., $f_M/f_c = 110\%$ [1], the number $K$ is far smaller than the number of antennas $N_t$, which is acceptable for hardware implementation.

By adopting the restriction of $K$ in (25), the array gain performance of the DDP can be derived. From (19), we have $|\eta(\bar{\mathbf{a}}_{l,m}, \theta_{l,m})| = \frac{K}{N_t}\left|\Xi_P(\frac{\bar{\beta}_{l,m}}{P})\right|$. Notice that $\bar{\beta}_{l,m} = (\xi_m - 1)P\theta_{l,c}$, $\theta_{l,m} = \xi_m\theta_{l,c}$ and $\theta_{l,c} \in [-1, 1]$, we have

$$\mathbb{E}(|\eta(\bar{\mathbf{a}}_{m,l}, \theta_{l,m})|) = \frac{K}{2MN_t}\sum_{m=1}^{M}\int_{-1}^{1}|\Xi_P((\xi_m - 1)\theta_{l,c})|\mathrm{d}\theta_{l,c}. \tag{26}$$

Because the integration of the Dirichlet sinc function is hard to computed [13], we utilize a polynomial to fit it by three points $(-1, |\Xi_P(1-\xi_m)|)$, $(0, P)$ and $(1, |\Xi_P(\xi_m - 1)|)$ as

$$\begin{aligned} &\int_{-1}^{1}|\Xi_P((\xi_m - 1)\theta_{l,c})|\mathrm{d}\theta_{l,c} \\ &\approx \int_{-1}^{1}\left[(\Xi_P(\xi_m - 1) - P)\theta_{l,c}^2 + P\right]\mathrm{d}\theta_{l,c}. \end{aligned} \tag{27}$$

By substituting (27) into (26), we have

$$\mathbb{E}(|\eta(\bar{\mathbf{a}}_{m,l}, \theta_{l,m})|) \approx \frac{K}{MN_t}\sum_{m=1}^{M}\left(\frac{1}{3}|\Xi_P(\xi_m - 1)| + \frac{2}{3}P\right). \tag{28}$$

(28) indicates that the expectation of the array gain achieved by the DPP is decided by the relative frequency $\xi_m$ and $K$. Considering the constraint of (25), $\xi_m - 1$ always locates in the main lobe of the Dirichlet sinc function $\Xi_P(x)$. This guarantees the array gain of the DDP is larger than $\frac{2KP}{3N_t} = 0.667$, which is much better than the array gain of the traditional structure shown in Fig. 2. Specifically, When $f_c = 100$ GHz, $f = 5$ GHz, $M = 128$, $K = 8$ and $N_t = 256$, we have $\mathbb{E}(|\eta(\bar{\mathbf{a}}_{m,l}, \theta_{l,m})|) \approx 0.96$, which means the proposed DPP is able to approach near-optimal array gain at all the subcarriers and the beam split effect can be efficiently relieved.

## V. Simulation Results

In this section, numerical simulation results are shown to verify the performance of the proposed DPP. The system parameters are: $N_t = 256$, $N_r = N_s = 4$, $M = 128$, $N_{RF} = 4$, $K = 8$, $f_c = 100$ GHz, $f = 5$ GHz, $L = 4$, and $\bar{\theta}_l, \bar{\phi}_l \sim \mathcal{U}[-\pi/2, \pi/2]$.

Fig. 5 shows the beam pattern and the array gain of the proposed DPP with $\theta_{l,c} = 0.5$. We can observe from Fig. 5 (a) and (b) that the beam is changed to be aligned with spatial direction $\theta_{l,m}$ at $f_1$ and $f_M$. Meanwhile, in Fig. 5 (b), the beams generated by the proposed DPP can achieve nearly 95% highest array gain at $f_1$ and $f_M$, which is consistent with the array gain analysis in IV. Moreover, we can see from Fig.

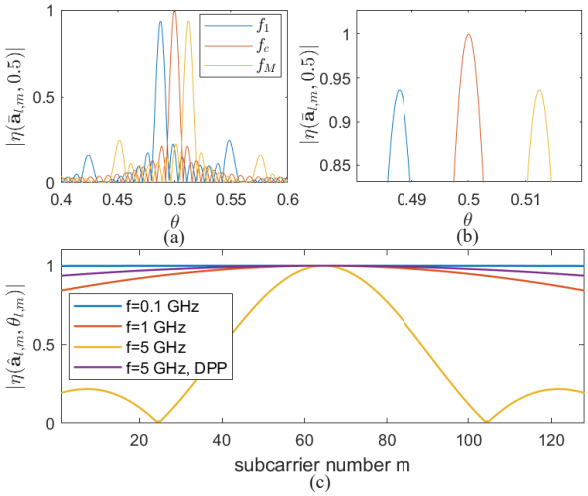


Fig. 5. (a) beam pattern of $\bar{\mathbf{a}}_{l,m}$ realized by the proposed DPP; (b) Enlarged version of Fig. 5 (a); (c) array gain comparison of $\bar{\mathbf{a}}_{l,m}$ and $\mathbf{a}_l$.

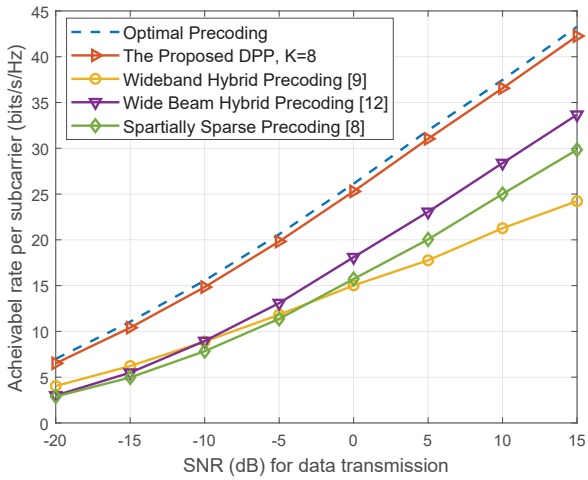


Fig. 6. The achievable rate performance comparison.

5 (c) that the proposed DPP with $K = 8$ can realize almost flat array gain over the whole bandwidth with $f = 5$ GHz, even better than that of the phase-controlled beam $\mathbf{a}_l$ with $f = 1$ GHz. We can conclude from Fig. 5 that the proposed DPP can near-optimally relieve the beam split effect.

Fig. 6 shows the achievable rate performance comparison between the proposed DPP and other existing methods, including wideband hybrid precoding with optimization [9], spatially sparse precoding [8] and wide beam based hybrid precoding [12], which are based on traditional frequency-independent PSs. We utilize the following equation to calculate the achievable rate performance as $R = \frac{1}{M}\sum_{m=1}^{M} \log_2\left(\left|\mathbf{I}_{N_s} + \frac{\rho}{N_s\sigma^2}\mathbf{H}\mathbf{A}_m\mathbf{D}_m\mathbf{D}_m^H\mathbf{A}_m^H\mathbf{H}^H\right|\right)$, in which the signal-to-noise ratio (SNR) is defined as $\rho/\sigma^2$, and $\mathbf{A}_m = \mathbf{A}$ in (1) for traditional structure [8], [9], [12], $\mathbf{A}_m = \mathbf{A}_u\mathbf{A}_m^{TD}$ in (11) for the DPP. We can observe from Fig. 6 that the proposed DPP outperforms the other methods and can achieve over 95% performance of the benchmark, the optimal unconstraint full-digital precoding, due to the jointly delay-phase controlled beamformer. Thus, the DPP can solve the achievable rate degradation incurred by the beam split effect and achieve near-optimal achievable rate performance.

## VI. Conclusions

In this paper, we investigate the wideband hybrid precoding in THz massive MIMO. A vital problem called beam split effect, where the path components split according to subcarrier frequencies, is analyzed. We point out that beam split effect may cause serious array gain loss and achievable rate decline in THz massive MIMO. To solve this problem, we propose a DPP structure where a TD network is introduced to compensate for the beam split through jointly delay-phase controlled beamformer. Theoretical analysis and simulation results show that the proposed DPP can eliminate the beam split with near-optimal array gain and achievable rate performance.

## Acknowledgments

This work was supported in part by the National Science and Technology Major Project of China under Grant 2018ZX03001004-003, in part by the National Natural Science Foundation of China for Outstanding Young Scholars under Grant 61722109, and in part by the National Natural Science Foundation of China under Grant 61571270.

## References

[1] I. F. Akyildiz, J. M. Jornet, and C. Han, "Terahertz band: Next frontier for wireless communications," *Phys. Commun.*, vol. 12, no. 2, pp. 16–32, Sep. 2014.

[2] S. Mumtaz, J. Rodriquez, and L. Dai, *MmWave Massive MIMO: A Paradigm for 5G*. Academic Press, Elsevier, 2016.

[3] H. Song and T. Nagatsuma, "Present and future of terahertz communications," *IEEE Trans. THz Sci. Technol.*, vol. 1, no. 1, pp. 256–263, Sep. 2011.

[4] X. Gao, L. Dai, Y. Zhang, T. Xie, X. Dai, and Z. Wang, "Fast channel tracking for terahertz beamspace massive MIMO systems," *IEEE Trans. Veh. Technol.*, vol. 66, no. 7, pp. 5689–5696, Jul. 2017.

[5] J. A. Zhang, X. Huang, V. Dyadyuk, and Y. J. Guo, "Massive hybrid antenna array for millimeter-wave cellular communications," *IEEE Wireless Commun.*, vol. 22, no. 1, pp. 79–87, Feb. 2015.

[6] X. Gao, L. Dai, and A. M. Sayeed, "Low RF-complexity technologies to enable millimeter-wave MIMO with large antenna array for 5G wireless communications," *IEEE Commun. Mag.*, vol. 56, no. 4, pp. 211–217, Apr. 2018.

[7] C. Han and Y. Chen, "Propagation modeling for wireless communications in the terahertz band," *IEEE Commun. Mag.*, vol. 56, no. 6, pp. 96–101, Jun. 2018.

[8] O. E. Ayach, S. Rajagopal, S. Abu-Surra, Z. Pi, and R. W. Heath, "Spatially sparse precoding in millimeter wave MIMO systems," *IEEE Trans. Wireless Commun.*, vol. 13, no. 3, pp. 1499–1513, Mar. 2014.

[9] S. Park, A. Alkhateeb, and R. W. Heath, "Dynamic subarrays for hybrid precoding in wideband mmwave MIMO systems," *IEEE Trans. Wireless Commun.*, vol. 16, no. 5, pp. 2907–2920, May 2017.

[10] L. Kong, S. Han, and C. Yang, "Hybrid precoding with rate and coverage constraints for wideband massive MIMO systems," *IEEE Trans. Wireless Commun.*, vol. 17, no. 7, pp. 4634–4647, Jul. 2018.

[11] M. Cai, K. Gao, D. Nie, B. Hochwald, J. N. Laneman, H. Huang, and K. Liu, "Effect of wideband beam squint on codebook design in phased-array wireless systems," in *Proc. IEEE GLOBECOM 2016*, Dec. 2016, pp. 1–6.

[12] X. Liu and D. Qiao, "Space-time block coding-based beamforming for beam squint compensation," *IEEE Wireless Commun. Lett.*, vol. 8, no. 1, pp. 241–244, Feb. 2019.

[13] R. J. Mailloux, *Phased Array Antenna Handbook*. Norwood, MA, USA: Artech House, 2005.

[14] Z. Xiao, P. Xia, and X. Xia, "Channel estimation and hybrid precoding for millimeter-wave MIMO systems: A low-complexity overall solution," *IEEE Access*, vol. 5, pp. 16 100–16 110, Jul. 2017.

[15] H. Hashemi, T. Chu, and J. Roderick, "Integrated true-time-delay-based ultra-wideband array processing," *IEEE Commun. Mag.*, vol. 46, no. 9, pp. 162–172, Sep. 2008.